https://dx.doi.org/10.1016/j.jmps.2022.104783

A generalized solution to the combo-crack problem—I. Pressure load on crack surface

Haimin Yao*, Chong Zhang

Department of Mechanical Engineering, The Hong Kong Polytechnic University, Hung Hom, Kowloon, Hong Kong SAR, China

*To whom correspondence should be addressed, E-Mail: mmhyao@polyu.edu.hk (H. Yao)

Abstract:

The axisymmetric elasticity problem of crack combo containing an externally circular crack (ECC) and a coplanar concentric penny-shaped crack (PSC) is mathematically equivalent to the annular contact problem. This problem has been attempted by using Love's strain potential approach, which eventually comes down to solving a pair of simultaneous Fredholm integral equations. Finding the closed-form solutions to the integral equations is difficult, if not impossible. Approximate solutions have been proposed in power series representations, which suffer from two major deficiencies. First, the solutions apply only to a special loading case in which uniform pressure is applied to the whole surface of the interior PSC. Secondly, the accuracy of the solution becomes unsatisfactory when the interior PSC tip is close to the ECC tip. To address these issues, in this paper we revisit this problem by considering a more general loading case in which uniform pressure is applied to a circular region of any size at the center of the PSC's surface. To overcome the lower accuracy caused by power series with limited terms, we numerically solve the pair of simultaneous Fredholm integral equations based on the *Gauss-Lobatto* quadrature. The high accuracy of our solution in the whole size spectra of the PSC and ECC is verified by finite element simulations. Our paper provides a generalized and more accurate solution to the annular contact problem or the combo crack problem, which deserves to be included in the updated library of the solutions to basic crack problems.

Keywords:

Fredholm integral equation; Stress intensity factor; *Gauss-Lobatto* quadrature; Hankel transform; Annular contact problem

1. Introduction

In linear elastic fracture mechanics (LEFM), the penny-shaped crack (PSC) and externally circular crack (ECC), as two basic axisymmetric crack configurations in a three-dimensional medium, have been well studied (Barenblatt, 1962; Sneddon, 1946, 1951). For both problems, closed-form solutions to the stress intensity factors (SIFs) under regular loading are present and well archived in the solution handbook of cracks (Tada et al., 2000). However, when an elastic solid contains both PSC and ECC, finding the closed-form solutions to the SIFs at the crack tips turns to be quite challenging, if not impossible, even though the PSC and ECC are coplanar and concentric and the load is uniform and symmetric (see Figure 1a). It is noteworthy that such a combo crack problem is mathematically equivalent to the annular contact problem, in which an elastic half-space is in adhesive and frictionless contact with a rigid substrate through an annular ligament (see Figure 1b). Therefore, in our discussion below we do not distinguish them unless stated otherwise.

As a typical axisymmetric elasticity problem, the combo crack problem depicted in Figure 1 has been attempted by researchers using Love's strain potential approach (Gladwell, 1980; Sneddon, 1951), resulting in a pair of simultaneous Fredholm integral equations. Finding the closed-form solution to the simultaneous integral equations is mathematically difficult and probably impossible. Selvaduri and Singh proposed an approximate solution by using power series representations (Selvadurai and Singh, 1987). However, besides a missing factor of $2/\sqrt{\pi}$ in their solutions to the SIFs, their results have two major issues which significantly affect their application. First, the loading they considered was uniform pressure applied to the whole surface of the interior PSC. Secondly, significant error occurs when the tip of the interior PSC is close to that of the ECC (*e.g.*, $a \to b$ in Figure 1). This is essentially attributed to the limited terms of the truncated power series which fail to capture the singularity of the SIFs as two crack tips are getting closer. To address these issues, in this paper we revisit the combo crack problem by considering a more general loading case, in which the uniform pressure is applied to a circular region of any size at the center of the PSC surface (see Figure 1). Moreover, we simplify the pair of simultaneous Fredholm integral equations further to be a single inhomogeneous Fredholm integral equation of the second type, which can be easily solved by using a *Gauss-Lobatto* quadrature-based approach. Our attention in this paper is mainly focused on the SIFs at the tips of PSC and ECC. The remaining paper is structured as follows. In Section 2, we briefly introduce the Hankel transform-based representations of the solution to axisymmetric elasticity problems, whereby the present annular contact problem can be expressed as a pair of simultaneous Fredholm integral equations with mixed boundary conditions. Then, in Section 3 we follow the power series-based representation as proposed by Selvadurai and Singh (1987) to obtain the approximate solutions to the SIFs under the generalized loading case. To obtain more accurate solutions to the SIFs, in Section 4 we develop a *Gauss-Lobatto* quadrature-based approach to solve the problem. Finally, in Section 5, we apply the obtained solutions to predict the critical pressure load for breaking the annular bonded ligament and extend the solutions to more complex loading cases exemplified by the annular pressure load.

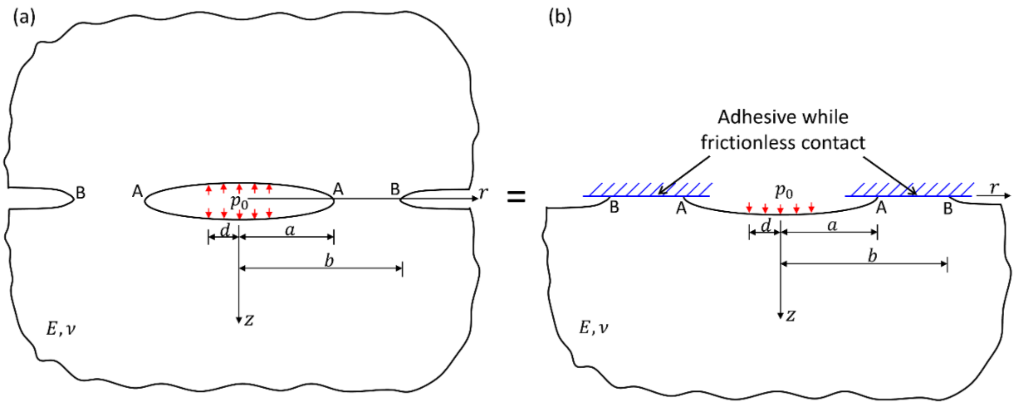

Figure 1. (a) Cross-sectional illustrations of the axisymmetric combo crack problem which contains an externally circular crack (ECC) of radius b embracing a coplanar concentric penny-shaped crack (PSC) of radius a. A self-balanced uniform pressure p_0 is applied to the central circular region of radius d on the surface of the PSC. (b) Cross-sectional illustration of the equivalent annular contact problem between an elastic half-space in adhesive and frictionless contact with a rigid substrate through an annular ligament region $(a \leq r \leq b)$. External uniform pressure load p_0 is applied to a circular region of radius d at the center of the interior free surface.

2. Hankel transform-based solution to axisymmetric half-space problems

In classical elasticity theory, the solution to an axisymmetric problem of a half-space, including the displacement components and Cauchy stress components, can be given in terms of a single biharmonic function called Love's strain function $\Phi(r, z)$ as (Gladwell, 1980)

$$2Gu_r = -\frac{\partial^2 \Phi}{\partial r \partial z} \tag{1a}$$

$$2Gu_z = 2(1-\nu)\nabla^2 \Phi - \frac{\partial^2 \Phi}{\partial z^2} \tag{1b}$$

$$\sigma_{rr} = \frac{\partial}{\partial r}\left\{\nu\nabla^2 \Phi - \frac{\partial^2 \Phi}{\partial r^2}\right\} \tag{2a}$$

$$\sigma_{\theta\theta}=\frac{\partial}{\partial z}\left\{\nu\nabla^2\Phi-\frac{1}{r}\frac{\partial\Phi}{\partial r}\right\} \tag{2b}$$

$$\sigma_{zz}=\frac{\partial}{\partial z}\left\{(2-\nu)\nabla^2\Phi-\frac{\partial^2\Phi}{\partial z^2}\right\} \tag{2c}$$

$$\sigma_{rz}=\frac{\partial}{\partial r}\left\{(1-\nu)\nabla^2\Phi-\frac{\partial^2\Phi}{\partial z^2}\right\} \tag{2d}$$

where G is shear modulus and $\nabla^2\equiv\frac{\partial^2}{\partial r^2}+\frac{1}{r}\frac{\partial}{\partial r}+\frac{\partial^2}{\partial z^2}$ is the axisymmetric form of *Laplace's* operator in a cylindrical polar coordinate system. By considering the condition that the stresses and displacement vanish at infinity ($z\to\infty$), it was demonstrated that the biharmonic Love's strain function should be given in the following form

$$\Phi(r,z)=\int_0^\infty\left[A_1(\xi)+zA_2(\xi)\right]e^{-\xi z}J_0(\xi r)\,d\xi \tag{3}$$

where $J_0(\cdot)$ is the 0-th order Bessel function of the first kind, $A_1(\xi)$ and $A_2(\xi)$ are two arbitrary functions to be determined according to the specific boundary conditions of the problem of interest. For any function $\psi(r)$, it can be demonstrated that (Yao, 2006)

$$\nabla^2\psi(r)=\frac{\partial^2\psi(r)}{\partial z^2}-H_0\left[\xi^2\Psi(\xi);\ \xi\to r\right],\ \ \Psi(\xi)=H_0\left[\psi(r);\ r\to\xi\right], \tag{4}$$

where $H_0[\psi(r);r\to\xi]\equiv\int_0^\infty r\psi(r)J_0(r\xi)dr$ represents the 0-th order Hankel's transform of function $\psi(r)$. Replacing $\psi(r)$ in Eq. (4) with $\Phi(r,z)$ given by Eq. (3) yields

$$\nabla^2\Phi=\frac{\partial^2\Phi}{\partial z^2}-\int_0^\infty\xi^2\left[A_1(\xi)+zA_2(\xi)\right]e^{-\xi z}J_0(\xi r)\,d\xi \tag{5}$$

Substituting Eqs. (3) and Eq. (5) into Eqs. (1b), (2c) and (2d) and then taking $z=0$, we have the normal displacement and stresses on the top surface of the half-space ($z=0$) as follows:

$$2Gu_z(r,0)=-\int_0^\infty\left[\xi^2A_1(\xi)+2(1-2\nu)\xi A_2(\xi)\right]J_0(\xi r)\,d\xi \tag{6a}$$

$$\sigma_{zz}(r,0)=\int_0^\infty\left[\xi^3A_1(\xi)+\xi^2(1-2\nu)A_2(\xi)\right]J_0(\xi r)\,d\xi \tag{6b}$$

$$\sigma_{rz}(r,0)=-\int_0^\infty\left[2\nu\xi^2A_2(\xi)-\xi^3A_1(\xi)\right]J_1(\xi r)\,d\xi \tag{6c}$$

In Eq. (6c), the relationship between the 0-th order and 1-st order Bessel functions, $\frac{\partial J_0(\xi r)}{\partial r} = -\xi J_1(\xi r)$, has been applied. Due to the frictionless contact in the contact problem (Figure 1b) or geometric symmetry about the plane of $z = 0$ in the crack problem (Figure 1a), the shear stress component (σ_{rz}) on the surface ($z = 0$) vanishes, which according to Eq. (6c) implies that

$$2\nu A_2(\xi) = \xi A_1(\xi) \tag{7}$$

Inserting Eq. (7) into Eqs. (6a) and (6b) yields

$$\frac{E^*}{2} u_z(r,0) = -\int_0^\infty \xi A_2(\xi) J_0(\xi r) d\xi = -H_0\left[A_2(\xi);\ \xi \to r\right] \tag{8a}$$

$$\sigma_{zz}(r,0) = \int_0^\infty \xi^2 A_2(\xi) J_0(\xi r) d\xi = H_0\left[\xi A_2(\xi);\ \xi \to r\right] \tag{8b}$$

where $E^* \equiv \frac{2G}{1-\nu} \equiv \frac{E}{1-\nu^2}$ is the plane-strain modulus of the material with E and ν being Young's modulus and Poisson's ratio, respectively. In the above equations, the unknown function $A_2(\xi)$ is to be determined by applying the mixed (displacement and normal stress) boundary conditions on the surface ($z = 0$) which, for the combo crack problem depicted in Figure 1, are given in terms of the following set of triple integral equations

$$\sigma_{zz}(r,0) = H_0\left[\xi A_2(\xi);\ \xi \to r\right] = f(r) = \begin{cases} -p_0, & (0 \le r \le d) \\ 0, & (d < r \le a) \end{cases} \tag{9a}$$

$$u_z(r,0) = -\frac{2}{E^*} H_0\left[A_2(\xi);\ \xi \to r\right] = 0, \quad (a \le r \le b) \tag{9b}$$

$$\sigma_{zz}(r,0) = H_0\left[\xi A_2(\xi);\ \xi \to r\right] = 0, \quad (b \le r < \infty) \tag{9c}$$

Similar equations have been obtained by Selvadurai and Singh (Selvadurai and Singh, 1987), in which the unknown function they used, $A(\xi)$, is related to our $A_2(\xi)$ through $A(\xi) = -\xi^2 A_2(\xi)$. To make an easy comparison with their results, in the following discussion, without loss of generality, we will replace $A_2(\xi)$ with $-\xi^{-2}A(\xi)$ and the triple integral equations above are rewritten as

$$H_0\left[\xi^{-1} A(\xi);\ \xi \to r\right] = f(r) = \begin{cases} p_0, & (0 \le r \le d) \\ 0, & (d < r \le a) \end{cases} \tag{10a}$$

$$H_0\left[\xi^{-2}A(\xi);\ \xi \to r\right]=0, \quad (a \le r \le b) \tag{10b}$$

$$H_0\left[\xi^{-1}A(\xi);\ \xi \to r\right]=0, \quad (b \le r < \infty) \tag{10c}$$

By following the same analytical techniques adopted by Selvadurai and Singh (1987), the above triple integral equations regarding the unknown function $A(\xi)$ can be converted to be a pair of simultaneous Fredholm integral equations (see **Appendix A** for detailed derivation)

$$F_1(s)+\frac{2s}{\pi}\int_b^{\infty}\frac{F_2(u)du}{(u^2-s^2)}=\begin{cases}-p_0 s, & (0\le s\le d)\\ -p_0\left[s-\left(s^2-d^2\right)^{1/2}\right], & (d\le s\le a)\end{cases} \tag{11a}$$

$$F_2(s)+\frac{2}{\pi}\int_0^{a}\frac{uF_1(u)du}{(s^2-u^2)}=0, \quad (b\le s<\infty) \tag{11b}$$

where $F_1(s)$ and $F_2(s)$ are two unknown functions defined in the domains of $s\in[0,a]$ and $s\in[b,\infty)$, respectively. If $F_1(s)$ and $F_2(s)$ are solved, the function $A(\xi)$ can be determined through

$$A(\xi)=\frac{2}{\pi}\xi^2\left[-\int_0^a F_1(s)\left\{\int_0^s\frac{rJ_0(\xi r)dr}{(s^2-r^2)^{1/2}}\right\}ds+\int_b^{\infty}F_2(s)ds\left\{\int_s^{\infty}\frac{rJ_0(\xi r)dr}{(r^2-s^2)^{1/2}}\right\}\right] \tag{12}$$

and the normal stress in the contact region of the surface ($z=0$) is given by[1]

$$\sigma_{zz}(r,0)=\frac{2}{\pi}\left[\frac{-F_1(a)}{(r^2-a^2)^{1/2}}+\int_0^a\frac{F_1'(s)ds}{(r^2-s^2)^{1/2}}+\frac{F_2(b)}{(b^2-r^2)^{1/2}}+\int_b^{\infty}\frac{F_2'(s)ds}{(s^2-r^2)^{1/2}}\right](a\le r\le b) \tag{13}$$

where $F_1'(s)$ and $F_2'(s)$ stand for the derivatives of functions $F_1'(s)$ and $F_2'(s)$ respectively.

The SIFs (mode I) at the crack tips of the PSC (point A) and ECC (point B) are given by

$$K_{\mathrm{A}}=\lim_{r\to a^+}\left[2\pi(r-a)\right]^{1/2}\sigma_{zz}(r,0)=-\frac{2}{\sqrt{a\pi}}F_1(a) \tag{14a}$$

$$K_{\mathrm{B}}=\lim_{r\to b^-}\left[2\pi(b-r)\right]^{1/2}\sigma_{zz}(r,0)=\frac{2}{\sqrt{b\pi}}F_2(b) \tag{14b}$$

By now, the original problem comes down to solving the simultaneous Fredholm integral equations of Eqs. (11a, 11b). For easy analysis and identification of the scaling law, we

[1] The expression of the normal stress σ_{zz} given by Selvadurai and Singh (1987) contained a couple of typos and missed a factor of $2/\pi$.

introduce nondimensional variables $\bar{u} \equiv u/b, \bar{s} \equiv s/a$ in Eqs. (11a) and $\bar{u} \equiv u/a, \bar{s} \equiv s/b$ in Eq. (11b). Both equations are thus normalized to be

$$\bar{F}_1(\bar{s}) + \frac{2c\bar{s}}{\pi}\int_1^{\infty}\frac{\bar{F}_2(\bar{u})d\bar{u}}{(\bar{u}^2-\bar{s}^2c^2)} = \begin{cases} -\bar{s}, & \left(0 \le \bar{s} \le \bar{d}\right) \\ -\bar{s} + \left(\bar{s}^2 - \bar{d}^2\right)^{1/2}, & \left(\bar{d} \le \bar{s} \le 1\right) \end{cases}$$

(15a)

$$\bar{F}_2(\bar{s}) + \frac{2c^2}{\pi}\int_0^1\frac{\bar{u}\bar{F}_1(\bar{u})d\bar{u}}{(\bar{s}^2-\bar{u}^2c^2)} = 0, \quad \left(1 \le \bar{s} < \infty\right) \tag{15b}$$

where $\bar{d} = d/a$, $c \equiv a/b$, $\bar{F}_1(\bar{s}) \equiv F_1(a\bar{s})/ap_0$, $\bar{F}_2(\bar{u}) \equiv F_2(b\bar{u})/ap_0$. The normal stress in the contact region and the SIFs can also be given in terms of the nondimensional functions

$$\sigma_{zz}(r,0) = \frac{2}{\pi}p_0\left[\frac{-a\bar{F}_1(1)}{(r^2-a^2)^{1/2}} + \int_0^1\frac{\bar{F}_1'(\bar{s})d\bar{s}}{(r^2/a^2-\bar{s}^2)^{1/2}} + \frac{a\bar{F}_2(1)}{(b^2-r^2)^{1/2}} + \frac{a}{b}\int_1^{\infty}\frac{\bar{F}_2'(\bar{s})d\bar{s}}{(\bar{s}^2-r^2/b^2)^{1/2}}\right] \tag{16}$$

$$K_{\mathrm{A}} = -\frac{2}{\sqrt{\pi}}\sqrt{a}\,p_0\bar{F}_1(1) \tag{17a}$$

$$K_{\mathrm{B}} = \frac{2}{\sqrt{\pi}}\sqrt{a}\,p_0\sqrt{c}\bar{F}_2(1) \tag{17b}$$

In the following, two different approaches will be applied to solve functions $\bar{F}_1(\bar{s})$ and $\bar{F}_2(\bar{s})$, followed by the determination of the SIFs K_{A} and K_{B} via Eqs. (17a) and (17b).

3. Power series-based approximate solution

Since function $\frac{1}{1-x}$ can be expanded in terms of the Taylor series at $x = 0$ as $\frac{1}{1-x} = 1 + x + x^2 + x^3 + \cdots$, the denominators of the integrands in Eqs. (15a) and (15b) thus can be written in terms of power series

$$\frac{1}{(\bar{u}^2-\bar{s}^2c^2)} = \frac{1}{\bar{u}^2}\frac{1}{(1-\bar{s}^2c^2/\bar{u}^2)} = \frac{1}{\bar{u}^2} + \frac{\bar{s}^2c^2}{\bar{u}^4} + \frac{\bar{s}^4c^4}{\bar{u}^6} + \frac{\bar{s}^6c^6}{\bar{u}^8} + \frac{\bar{s}^8c^8}{\bar{u}^{10}} + o(c^{10}) \tag{18a}$$

$$\frac{1}{(\bar{s}^2-\bar{u}^2c^2)} = \frac{1}{\bar{s}^2}\frac{1}{(1-\bar{u}^2c^2/\bar{s}^2)} = \frac{1}{\bar{s}^2} + \frac{\bar{u}^2c^2}{\bar{s}^4} + \frac{\bar{u}^4c^4}{\bar{s}^6} + \frac{\bar{u}^6c^6}{\bar{s}^8} + \frac{\bar{u}^8c^8}{\bar{s}^{10}} + o(c^{10}) \tag{18b}$$

Assuming $\bar{F}_1(\bar{s}) = \sum_{i=0}^{8} c^i m_i(\bar{s})$, $\bar{F}_2(\bar{s}) = \sum_{i=0}^{8} c^i n_i(\bar{s})$, Eqs. (15a)(15b) imply that

$$\sum_{i=0}^{8} c^i m_i(\bar{s}) + \frac{2\bar{s}}{\pi}\int_1^\infty \left[\frac{c}{\bar{u}^2}+\frac{\bar{s}^2c^3}{\bar{u}^4}+\frac{\bar{s}^4c^5}{\bar{u}^6}+\frac{\bar{s}^6c^7}{\bar{u}^8}+\frac{\bar{s}^8c^9}{\bar{u}^{10}}\right]\left[\begin{array}{l} n_0(\bar{u})+cn_1(\bar{u})+c^2n_2(\bar{u})+c^3n_3(\bar{u})+c^4n_4(\bar{u})+ \\ c^5n_5(\bar{u})+c^6n_6(\bar{u})+c^7n_7(\bar{u})+c^8n_8(\bar{u}) \end{array}\right] d\bar{u}$$
$$= \begin{cases} -\bar{s}, & \left(0 \le \bar{s} \le \bar{d}\right) \\ -\bar{s}+\left(\bar{s}^2-\bar{d}^2\right)^{1/2}, & \left(\bar{d} < \bar{s} \le 1\right) \end{cases}$$

$$\sum_{i=0}^{8} c^i n_i(\bar{s}) = -\frac{2}{\pi}\int_0^1 \bar{u}\left[\frac{c^2}{\bar{s}^2}+\frac{\bar{u}^2c^4}{\bar{s}^4}+\frac{\bar{u}^4c^6}{\bar{s}^6}+\frac{\bar{u}^6c^8}{\bar{s}^8}+\frac{\bar{u}^8c^{10}}{\bar{s}^{10}}\right]\left[\begin{array}{l} m_0(\bar{u})+cm_1(\bar{u})+c^2m_2(\bar{u})+c^3m_3(\bar{u})+c^4m_4(\bar{u}) \\ +c^5m_5(\bar{u})+c^6m_6(\bar{u})+c^7m_7(\bar{u})+c^8m_8(\bar{u}) \end{array}\right] d\bar{u}$$

By comparing the coefficients of like terms c^i on both sides of the above equations, functions $m_i(\bar{s})$ and $n_i(\bar{s})$ are determined (see **Appendix B** for the detailed expressions). Then, the SIFs at crack tips A and B are given by

$$K_{\mathrm{A}} = -\frac{2}{\sqrt{\pi}}\sqrt{a}\,p_0\bar{F}_1(1)$$

$$\begin{aligned} &= \frac{2}{\sqrt{\pi}}\sqrt{a}\,p_0\left\{\left(1-\sqrt{1-\bar{d}^2}\right)+\frac{4c^3}{9\pi^2}\phi_1\left(\bar{d}\right)+\frac{4c^5}{5\pi^2}\left[\frac{1}{5}\phi_2\left(\bar{d}\right)+\frac{1}{3}\phi_1\left(\bar{d}\right)\right]+\frac{16c^6}{81\pi^4}\phi_1\left(\bar{d}\right)\right. \\ &\left.+\frac{4c^7}{\pi^2}\left[\frac{1}{49}\phi_3\left(\bar{d}\right)+\frac{1}{35}\phi_2\left(\bar{d}\right)+\frac{1}{21}\phi_1\left(\bar{d}\right)\right]+\frac{16c^8}{\pi^4}\left[\frac{1}{75}\phi_6\left(\bar{d}\right)+\frac{1}{135}\phi_1\left(\bar{d}\right)\right]+o\left(c^9\right)\right\} \end{aligned} \quad (19a)$$

$$K_{\mathrm{B}} = \frac{2\sqrt{c}}{\sqrt{\pi}}\sqrt{a}\,p_0\bar{F}_2(1)$$

$$\begin{aligned} &= \frac{2}{\sqrt{\pi}}\sqrt{a}\,p_0\sqrt{c}\left\{\frac{2c^2}{3\pi}\phi_1\left(\bar{d}\right)+\frac{2c^4}{5\pi}\phi_2\left(\bar{d}\right)+\frac{8c^5}{27\pi^3}\phi_1\left(\bar{d}\right)+\frac{2c^6}{7\pi}\phi_3\left(\bar{d}\right)\right. \\ &\left.+\frac{16c^7}{\pi^3}\left[\frac{1}{75}\phi_4\left(\bar{d}\right)+\frac{1}{90}\phi_1\left(\bar{d}\right)\right]+\frac{2c^8}{9\pi}\left[\frac{16}{27\pi^4}\phi_1\left(\bar{d}\right)+\phi_5\left(\bar{d}\right)\right]+o(c^9)\right\} \end{aligned} \quad (19b)$$

where $\phi_i(\bar{d})$ $(i = 1,2,\cdots,6)$ are functions of $\bar{d}$ (see **Appendix B** for the detailed expressions).

Eqs. (19a) and (19b) provide power series-based approximate solutions to the SIFs for any $\bar{d} \in [0,1]$. As $\bar{d} \to 1$, the solutions above are reduced to those given by Selvadurai and Singh (1987). Figure 2 shows the variations of K_{A} and K_{B} with a/b (or c) for d/a =0.25, 0.5, 075, 1.0, respectively. It can be seen that $K_{\mathrm{A}} > K_{\mathrm{B}}$ irrespective of a/b, implying that the condition for crack propagation will be met first at the tip of PSC as the pressure load p_0 increases. Consequently, the interior PSC grows while the external crack keeps stationary always. To examine the accuracy of our results of the SIFs, we carried out finite element computations (ABAQUS, Dassault Systèmes) to calculate the SIFs numerically, as shown by the scattered symbols in Figure 2. Our series-based approximate solutions agree well with the FE results when $\frac{a}{b} < 0.7$. However, as $\frac{a}{b}$ increases further (*e.g.*, $\frac{a}{b} > 0.8$), our series solutions exhibit large deviations from the FE results which asymptotically approach infinity as $\frac{a}{b} \to 1.0$. Such singularity of the SIFs at $\frac{a}{b} \to 1$ is essentially attributed to the vanishing bonded area and therefore infinite stress at the limit of $\frac{a}{b} \to 1$. Increasing the number of the terms of the power series in Eqs.(18a) and (18b) can only defer the occurrence of such deviation of the solutions. To address this problem, an alternative approach to solving the simultaneous Fredholm integral equations in Eqs. (15a) and (15b) is developed.

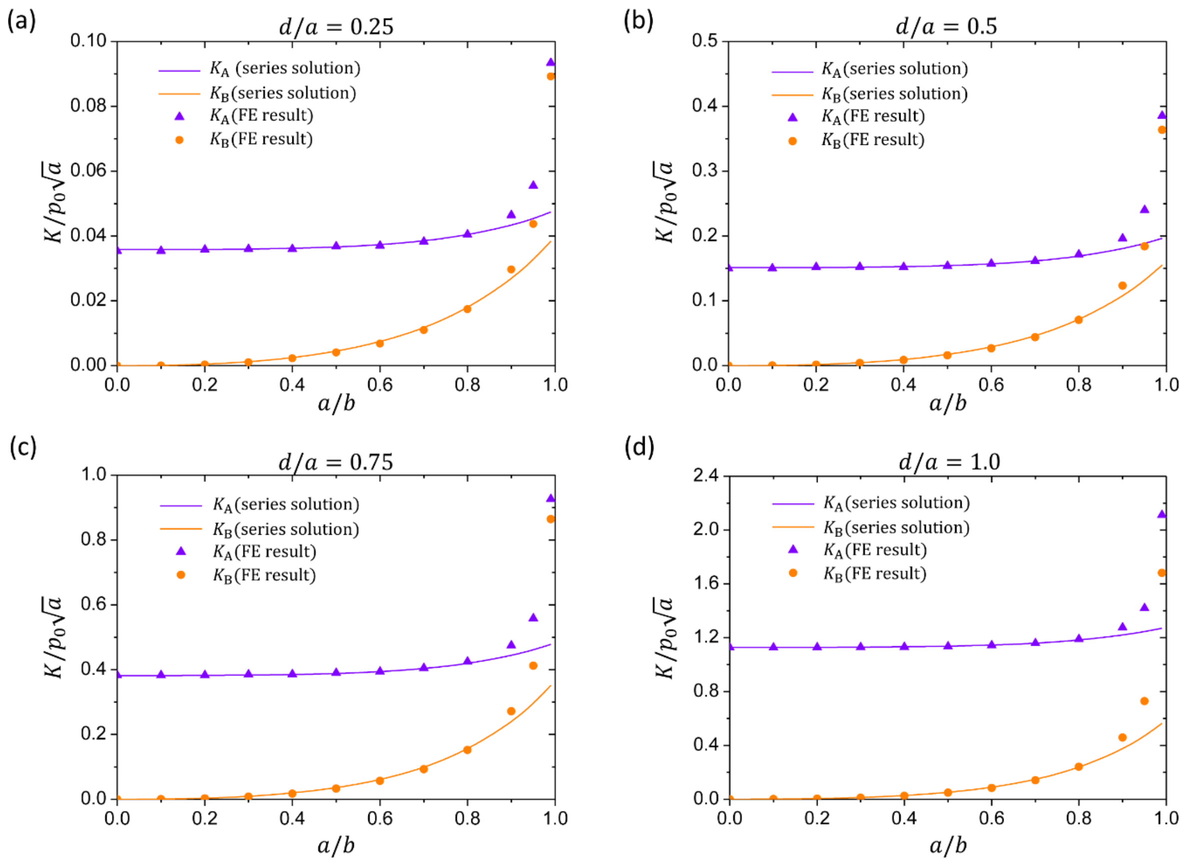

Figure 2. Series-based approximate solutions to the SIFs of the PSC (K_A) and the ECC (K_B) in comparison to the corresponding FE results for cases with (a) $d/a = 0.25$, (b) $d/a = 0.5$, (c) $d/a = 0.75$ and (d) $d/a = 1.0$.

4. Numerical quadrature-based solution

The integral in Eq. (15a) is defined in an infinite interval $[1, \infty)$. For the convenience of performing numerical integration, we substitute integration variable $\bar{u}$ by $1/t$ in Eq. (15a) and yields

$$\bar{F}_1(\bar{s}) + \frac{2c\bar{s}}{\pi}\int_0^1 \frac{\bar{F}_2(1/t)dt}{(1-t^2\bar{s}^2c^2)} = \bar{g}(\bar{s}) = \begin{cases} -\bar{s}, & \left(0 \le \bar{s} \le \bar{d}\right) \\ -\bar{s} + \left(\bar{s}^2 - \bar{d}^2\right)^{1/2}, & \left(\bar{d} < \bar{s} \le 1\right) \end{cases} \tag{20}$$

Meanwhile, from Eq. (15b) we have

$$\bar{F}_2(1/t) = -\frac{2c^2t^2}{\pi}\int_0^1 \frac{\bar{u}\bar{F}_1(\bar{u})d\bar{u}}{(1-t^2\bar{u}^2c^2)}, \quad (0<t\le 1) \tag{21}$$

Insertion of Eq.(21) into Eq.(20) to eliminate the unknown function $\bar{F}_2$ gives

$$\bar{F}_1(\bar{s}) - \frac{4c^3\bar{s}}{\pi^2}\int_0^1 t^2\left[\int_0^1 \frac{\bar{u}\bar{F}_1(\bar{u})d\bar{u}}{(1-t^2\bar{u}^2c^2)}\right]\frac{dt}{(1-t^2\bar{s}^2c^2)} = \bar{g}(\bar{s}), \quad (0\le\bar{s}\le 1) \tag{22}$$

Exchanging the order of two integrations in Eq. (22) gives rise to an inhomogeneous Fredholm integral equation of the second type

$$\bar{F}_1(\bar{s}) + \frac{2}{\pi^2}\int_0^1 \bar{Q}_1(\bar{u},\bar{s})\bar{F}_1(\bar{u})d\bar{u} = \bar{g}(\bar{s}), \quad (0\le\bar{s}\le 1) \tag{23}$$

where

$$\bar{Q}_1(\bar{u},\bar{s}) \equiv \left[\bar{u}\ln\left(\frac{1+\bar{s}c}{1-\bar{s}c}\right) - \bar{s}\ln\left(\frac{1+\bar{u}c}{1-\bar{u}c}\right)\right]\frac{1}{(\bar{u}^2-\bar{s}^2)}, \quad (0\le\bar{u}\le 1,\ 0\le\bar{s}\le 1) \tag{24}$$

is the symmetric kernel function. It can be demonstrated that $\lim_{\bar{u}\to\bar{s}} \bar{Q}_1(\bar{u},\bar{s}) = \frac{1}{2\bar{s}}\ln\left(\frac{1+\bar{s}c}{1-\bar{s}c}\right) + \frac{c}{c^2\bar{s}^2-1}$, which further approaches 0 as $\bar{s}\to 0$. Therefore, the kernel function $\bar{Q}_1(\bar{u},\bar{s})$ in Eq. (23) is nonsingular.

Although we have converted a pair of simultaneous Fredholm integral equations about two unknown functions $\bar{F}_1$ and $\bar{F}_2$ into a single inhomogeneous integral Fredholm equation about one single unknown function $\bar{F}_1$, finding its analytical solution remains challenging. In the following, a numerical approach is adopted to solve the unknown functions $\bar{F}_1$.

Substitution of $x = 2\bar{u} - 1$ in Eq. (23) changes the integration interval to $[-1, 1]$

$$\bar{F}_1(\bar{s}) + \frac{1}{\pi^2}\int_{-1}^1 \bar{Q}_1\left(\tfrac{x+1}{2},\bar{s}\right)\bar{F}_1\left(\tfrac{x+1}{2}\right)dx = \bar{g}(\bar{s}), \quad (0\le\bar{s}\le 1) \tag{25}$$

Applying the *Gauss-Lobatto* quadrature (Kovvali, 2013) to calculate the integration in Eq. (25) gives

$$\bar{F}_1(\bar{s}) + \frac{1}{\pi^2}\left\{\frac{2\left[\bar{Q}_1(0,\bar{s})\bar{F}_1(0) + \bar{Q}_1(1,\bar{s})\bar{F}_1(1)\right]}{n(n-1)} + \sum_{j=2}^{n-1} w_j\bar{Q}_1\left(\tfrac{x_j+1}{2},\bar{s}\right)\bar{F}_1\left(\tfrac{x_j+1}{2}\right)\right\} = \bar{g}(\bar{s}) \tag{26}$$

where n is the number of integration points and x_j $(j = 2, \cdots, n-1)$ are the integration points except ± 1 and w_j are the corresponding weights. In Eq. (26), taking $\bar{s}$ as values of $\bar{s}_1 = 0$,

$\bar{s}_i = \frac{x_i+1}{2}$ $(i = 2, \cdots, n-1)$ and $\bar{s}_n = 1$, we will obtain n equations about n unknown $\bar{F}_1\left(\frac{x_i+1}{2}\right)$ $(i = 1, \cdots, n)$. These equations can be written in a matrix form as follows:

$$(\mathbf{I} + \frac{1}{\pi^2}\mathbf{K})\bar{\mathbf{F}}_1 = \bar{\mathbf{g}} \tag{27}$$

where $\mathbf{I}$ is the $n \times n$ unit matrix and

$$\mathbf{K} = \begin{bmatrix} \frac{2\bar{Q}_1(0,0)}{n(n-1)} & \cdots & w_j\bar{Q}_1\left(\frac{x_j+1}{2},0\right) & \cdots & \frac{2\bar{Q}_1(1,0)}{n(n-1)} \\ \vdots & \vdots & \vdots & \vdots & \vdots \\ \frac{2\bar{Q}_1\left(0,\frac{x_i+1}{2}\right)}{n(n-1)} & \cdots & w_j\bar{Q}_1\left(\frac{x_j+1}{2},\frac{x_i+1}{2}\right) & \cdots & \frac{2\bar{Q}_1\left(1,\frac{x_i+1}{2}\right)}{n(n-1)} \\ \vdots & \vdots & \vdots & \vdots & \vdots \\ \frac{2\bar{Q}_1(0,1)}{n(n-1)} & \cdots & w_j\bar{Q}_1\left(\frac{x_j+1}{2},1\right) & \cdots & \frac{2\bar{Q}_1(1,1)}{n(n-1)} \end{bmatrix}_{n\times n} \quad \bar{\mathbf{F}}_1 = \begin{bmatrix} \bar{F}_1(0) \\ \vdots \\ \bar{F}_1(\frac{x_j+1}{2}) \\ \vdots \\ \bar{F}_1(1) \end{bmatrix}_{n\times 1} \quad \bar{\mathbf{g}} = \begin{bmatrix} \bar{g}(0) \\ \vdots \\ \bar{g}(\frac{x_i+1}{2}) \\ \vdots \\ \bar{g}(1) \end{bmatrix}_{n\times 1}$$

Solving Eq. (27) for the unknown array $\bar{\mathbf{F}}_1$ by left multiplying the inverse matrix of $(\mathbf{I} + \frac{1}{\pi^2}\mathbf{K})$ on both sides of Eq. (27) gives rise to

$$\bar{\mathbf{F}}_1 = (\mathbf{I} + \frac{1}{\pi^2}\mathbf{K})^{-1}\bar{\mathbf{g}} \tag{28}$$

Then, applying *Gauss-Lobatto* quadrature in Eq. (15b) with the obtained $\bar{F}_1\left(\frac{x_i+1}{2}\right)$ gives

$$\bar{F}_2(\bar{s}) = -\frac{c^2}{\pi}\left[\frac{2}{n(n-1)}\left[\bar{Q}_2(0,\bar{s})\bar{F}_1(0) + \bar{Q}_2(1,\bar{s})\bar{F}_1(1)\right] + \sum_{j=2}^{n-1}\omega_j\bar{Q}_2(\frac{x_j+1}{2},\bar{s})\bar{F}_1(\frac{x_j+1}{2})\right] \tag{29}$$

where $\bar{Q}_2\left(\frac{x+1}{2},\bar{s}\right) \equiv \frac{(x+1)/2}{[\bar{s}^2-(x+1)^2c^2/4]}$ and x_j $(j = 2, \cdots, n-1)$ are the integration points except ± 1 and w_j are the corresponding weights. The SIFs at the crack tips A and B thereby are determined via $K_{\mathrm{A}} = -\frac{2}{\sqrt{\pi}}\sqrt{a}p_0\bar{F}_1(1)$, $K_{\mathrm{B}} = \frac{2}{\sqrt{\pi}}\sqrt{a}p_0\sqrt{c}\bar{F}_2(1)$. The above algorithm can be easily implemented with MATLAB (R2015a, The MathWorks Inc.). Figure 3 shows the results we calculated by adopting 50 integration points in comparison with the FE results (ABAQUS, Dassault Systèmes). Further increase of the integration points will not bring too much changes to the results. It can be seen that our numerical quadrature-based solutions agree with the FE results very well, implying that this approach successfully captures the featured singularity of SIFs as $a/b \to 1.0$. Moreover, the SIFs especially that at the tip of the interior PSC vary little with the ratio of a/b in the range of $0 < a/b < 0.6$, but its value strongly relys on the size of the load region (d) which determines the net force load. As expected, when $b \to \infty$ (or $a/b \to$

0), our numerical solution to K_{A} is reduced to the solution of a single penny-shaped crack case, which can be analytically expressed as $K = \frac{2p_0\sqrt{a}}{\sqrt{\pi}}\left(1-\sqrt{1-d^2/a^2}\right)$ (Tada et al., 2000).

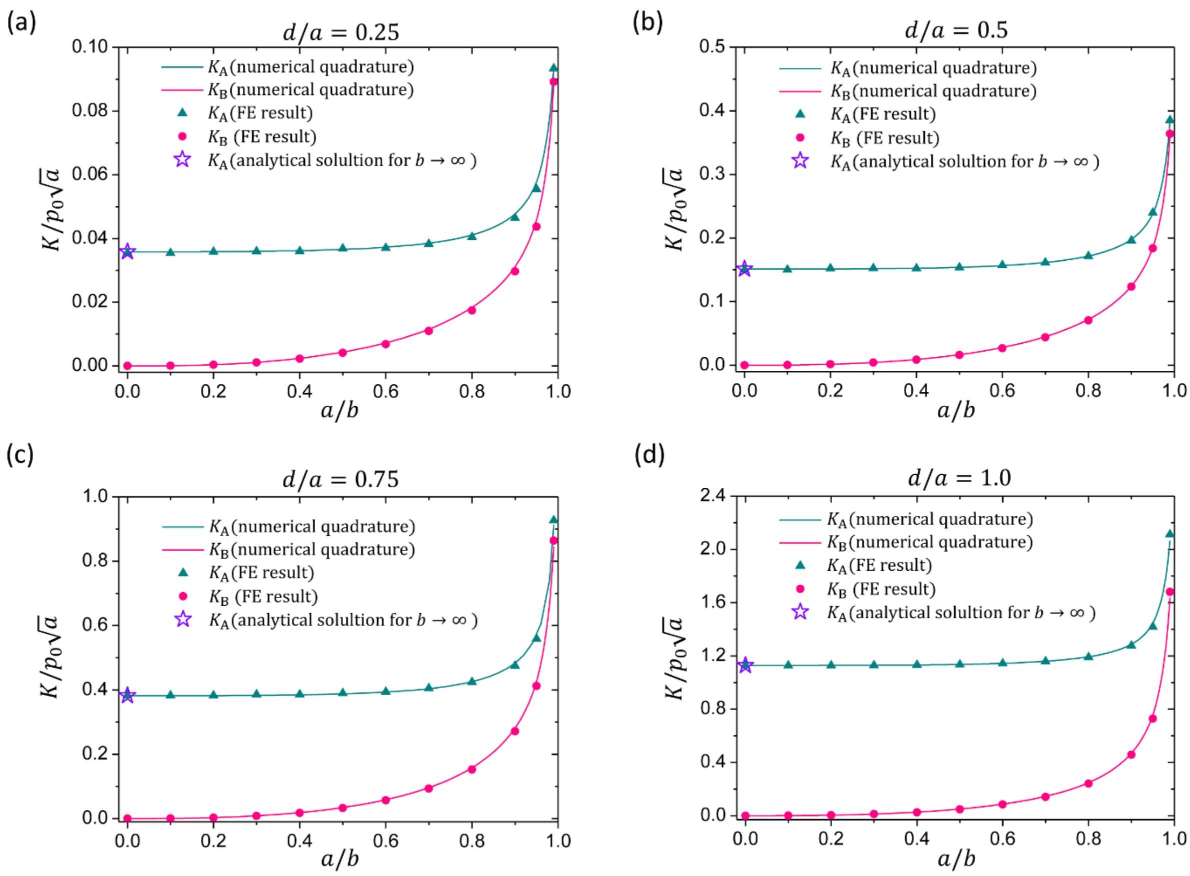

Figure 3. Numerical quadrature-based solutions to the SIFs at the PSC tip (K_{A}) and the ECC tip (K_{B}) in comparison to the FE results for cases with (a) $d/a = 0.25$, (b) $d/a = 0.5$, (c) $d/a = 0.75$ and (d) $d/a = 1.0$. The hollow star symbols represent the analytical solution for the limiting case ($b \to \infty$) in which $K/p_0\sqrt{a} = \frac{2}{\sqrt{\pi}}\left(1-\sqrt{1-d^2/a^2}\right)$.

5. Discussion and conclusion

Our preceding results show that the normalized SIFs ($K/p_0\sqrt{a}$) at tips of the PSC and ECC depend on two independent nondimensional parameters, which are chosen as $\frac{a}{b}$ and $\frac{d}{a}$ in Figure 3. It can be seen that in the whole spectra of both parameters ($0 < \frac{a}{b} < 1.0$, $0 < \frac{d}{a} \leq 1.0$), the SIF at the PSC tip (K_{A}) is always higher than that at the ECC tip (K_{B}), implying that breakage of the bonded ligament, if happens, should start from the interior PSC while the ECC tip keeps stationary always. During this process, the radius of the PSC (a) is increasing while the radius of the ECC (b) remains constant. To examine the variation of SIF at the PSC tip with the increasing crack size, we adopt the radius of the load region (d) as an alternative length scale for normalization. The normalized SIF at the PSC tip ($\bar{K}_{\mathrm{A}} \equiv K_{\mathrm{A}}/p_0\sqrt{d}$) is shown in Figure 4a as a function of two normalized crack sizes $\bar{a} \equiv a/d$ and $\bar{b} \equiv b/d$. For a given $\bar{b}$, the stress intensity factor $\bar{K}_{\mathrm{A}}$ initially decreases and then increases as $\bar{a}$ varies from 1 to $\bar{b}$, as shown in Figure 4b. There exists a critical $\bar{a}$, at which $\left(\frac{\partial \bar{K}_{\mathrm{A}}}{\partial \bar{a}}\right)_{\bar{b}} = 0$ and $\bar{K}_{\mathrm{A}}$ reaches the least value for that given $\bar{b}$. Griffith's criterion (Griffith, 1921) for crack propagation indicates that crack will propagate when the SIF reaches a critical value of $K_{\mathrm{c}} \equiv \sqrt{E'\Delta\gamma}$, where modulus $E' = 2E^*$ and $\Delta\gamma$ is the work of adhesion[2] (Israelachvili, 1992). Equating K_{A} with $\sqrt{E'\Delta\gamma}$ determines the equilibrium pressure (p_0^{eq}) as a function of $\bar{a}$ and $\bar{b}$, as shown in Figure 4c in a normalized fashion. As expected, for a given $\bar{b}$ the normalized equilibrium pressure ($\bar{p}_0^{\mathrm{eq}}$) initially increases and then decrease with the increasing $\bar{a}$, as shown in Figure 4d. At the critical $\bar{a}$, $\left(\frac{\partial \bar{p}_0^{\mathrm{eq}}}{\partial \bar{a}}\right)_{\bar{b}} = 0$ and p_0^{eq} reaches its peak value denoted by p_{pf} . This peak pressure is called *push-off pressure* because the equilibrium state after this moment is unstable and catastrophic fracture between two solids would happen spontaneously. The push-off pressure and the corresponding radius of the PSC (a_{pf}) depend on the radius of ECC, as shown in Figure 4e and Figure 4f, respectively. Interestingly, a_{pf} exhibits an almost linear proportionality to b , implying that the catastrophic fracture happens at an almost constant ratio of $a/b \approx 0.87$ unless b is quite close to d (*e.g.*, $b/d < 1.5$), as shown by the second *y*-axis in Figure 4f.

[2] For an analogous crack problem shown in Figure 1a, $E' = E^*$ and $\Delta\gamma$ is fracture toughness of the material.

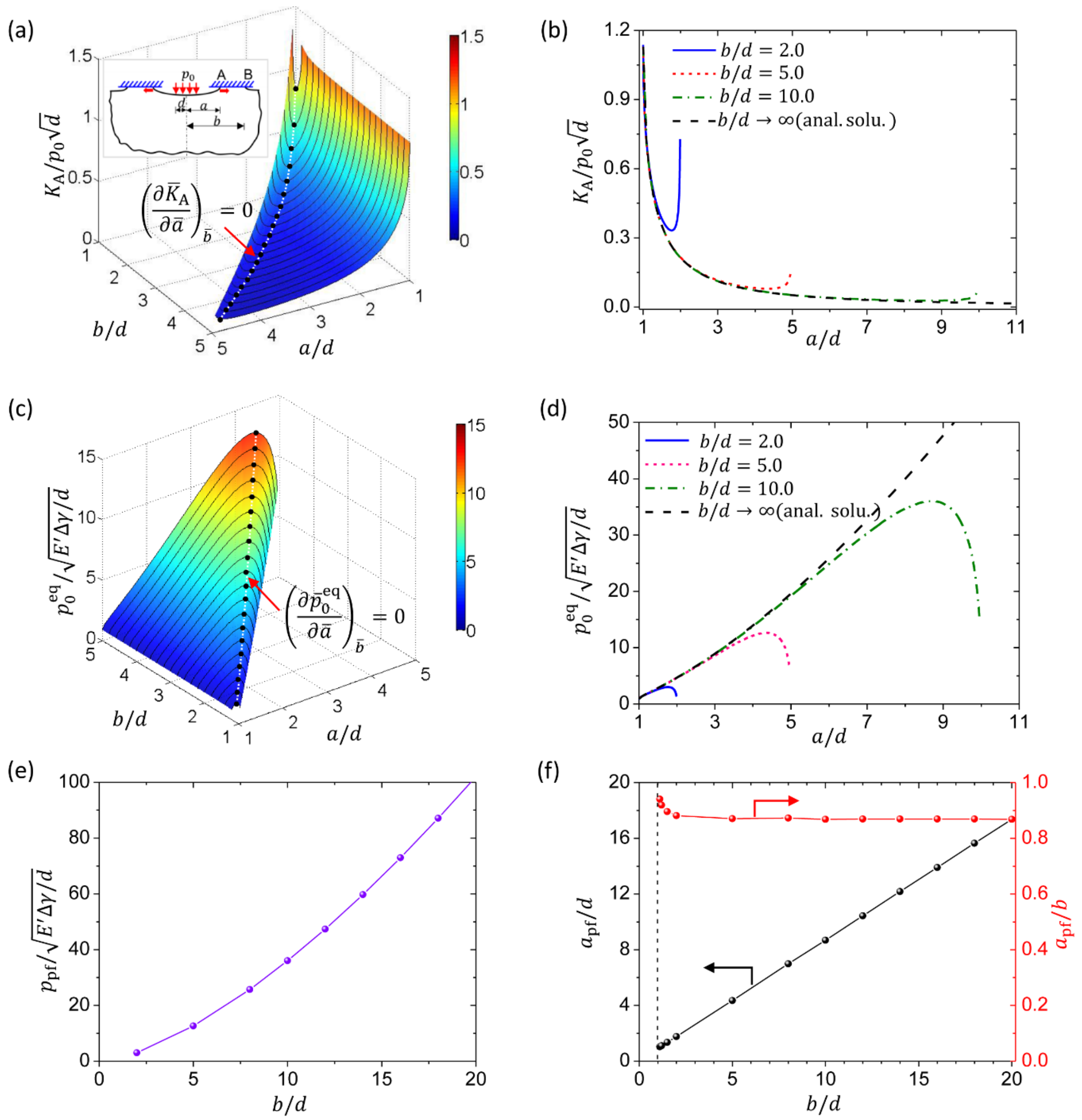

Figure 4. (a) Dependence of the normalized SIF at the PSC tip ($\bar{K}_A \equiv K_A/p_0\sqrt{d}$) on the normalized crack radii ($\bar{a} \equiv a/d$) and $\bar{b} \equiv b/d$. The black profile curves on the 3D surface depict the evolution of $\bar{K}_A$ with $\bar{a}$ for given values of $\bar{b}$. The while dash line indicates the point at which $\left(\frac{\partial \bar{K}_A}{\partial \bar{a}}\right)_{\bar{b}} = 0$. (b) Calculated variaitons of $\bar{K}_A$ with $\bar{a}$ for $\bar{b} = 2.0, 5.0, 10.0$ in comparison with the analytical solution of the limiting case ($b \to \infty$) in which $K_A/p_0\sqrt{d} = \frac{2}{\sqrt{\pi}}\left(\sqrt{a/d} - \sqrt{a/d - d/a}\right)$. (c) Dependence of the normalized equilibrium pressure ($\bar{p}_0^{eq} \equiv p_0^{eq}/\sqrt{E'\Delta\gamma/d}$) on the normalized crack radii ($\bar{a} \equiv a/d$) and $\bar{b} \equiv b/d$. The black profile curves on the 3D surface depict the evolution of $\bar{p}_0^{eq}$ with $\bar{a}$ for given values of $\bar{b}$. The while dash line indicates the point at which $\left(\frac{\partial \bar{p}_0^{eq}}{\partial \bar{a}}\right)_{\bar{b}} = 0$. (d) Calculated variaitons of $\bar{p}_0^{eq}$ with $\bar{a}$ for $\bar{b} = 2.0, 5.0, 10.0$ in comparison with the analytical solution of the limiting case ($b \to \infty$) in which $\bar{p}_0^{eq} = \frac{\sqrt{\pi}}{2}\left(\sqrt{a/d} - \sqrt{a/d - d/a}\right)^{-1}$. (e) Variation of the normalized push-off

pressure ($\bar{p}_{\mathrm{pf}} \equiv p_{\mathrm{pf}}/\sqrt{E'\Delta\gamma/d}$) with the normalized radius of the ECC (b/d). (f) Variations of the radius of PSC at the push-off moment and its ratio to the radius of ECC with b/d.

Although our solutions to the SIFs are developed only for the uniform pressure applied to a circular region ($0 \le r \le d \le a$), we can apply the results to calculate the SIFs for other complex loading cases by using the superposition method. For example, the SIFs caused by uniform pressure p_0 applied to an annular region ($d \le r \le a$) (see Figure 5a), which are denoted by K'_{A} and K'_{B}, can be obtained through

$$K'_{\mathrm{A/B}} = p_0\sqrt{d}\left[\sqrt{\frac{a}{d}}\bar{K}_{\mathrm{A/B}}\left(1.0, \frac{b}{a}\right) - \bar{K}_{\mathrm{A/B}}\left(\frac{a}{d}, \frac{b}{d}\right)\right] \tag{30}$$

where $\bar{K}_{\mathrm{A/B}}\left(\frac{a}{d}, \frac{b}{d}\right)$ represents the normalized SIF at point A or B caused by pressure applied to the circular region $0 \le r \le d$ and $\bar{K}_{\mathrm{A/B}}\left(1.0, \frac{b}{a}\right)$ represents its value at $\frac{a}{d} = 1.0$. Figures 5b shows the variations of $K'_{\mathrm{A/B}}$ with $\frac{a}{d}$ for selected values of $\frac{b}{d} = 2.0, 5.0, 10.0$ together with the analytical solution to K'_{A} for the limiting case of $b \to \infty$ (Tada et al., 2000). It can be seen that for a given $\bar{b}$, both SIFs increase monotonically with $\bar{a}$. When $\frac{a}{d} < 0.7$, the ECC has little effect on K'_{A}. The panoramic dependences of the $\bar{K}'_{\mathrm{A}}$ and $\bar{K}'_{\mathrm{B}}$ on $\frac{a}{d}$ and $\frac{b}{d}$ are shown in Figure 5c and Figure 5d, respectively. Once again, under annular pressure load, the SIF at the PSC tip is also higher than that at the ECC tip, irrespective of the values of $\frac{a}{d}$ and $\frac{b}{d}$.

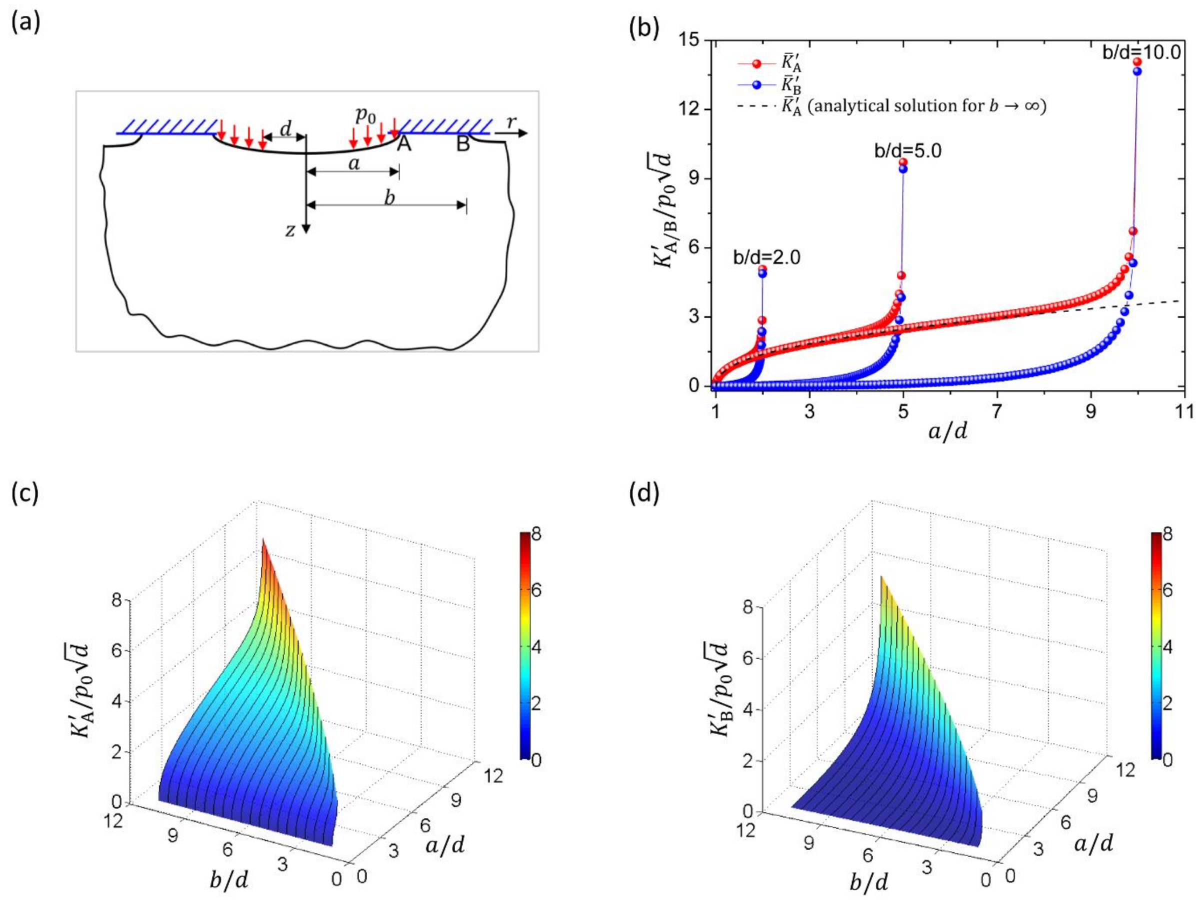

Figure 5. (a) Illustration showing the case with uniform pressure load p_0 applied to an annular region ($d \leq r \leq a$) on the surface of PSC. (b) Variations of the SIFs caused by annular pressure load with b/d for selected $b/d = 2.0$, 5.0, 10.0 in comparison with the analytical solution for the limiting case ($b \to \infty$) when $K'_A/p_0\sqrt{d} = \frac{2}{\sqrt{\pi}}\sqrt{a/d - d/a}$. (c-d) Dependences of the SIFs $\bar{K}'_A$ and $\bar{K}'_B$ caused by annular pressure load on a/d and b/d. The profile curves on the 3D surfaces depict the evolution of $\bar{K}'_{A/B}$ with $\bar{a}$ for given values of $\bar{b}$.

To summarize, in this paper we revisited the classical combo crack problem which is mathematically equivalent to the annular contact problem. Our attention was mainly focused on the SIFs at both crack tips. On the top of the existing results especially the power series-based solution to the problem, we made two major extensions. First, we considered a more general loading case, in which uniform pressure load is applied to a circular region of any size at the center of the PSC surface. More importantly, we developed a numerical quadrature-based technique, which enabled us to obtain more accurate results of the SIFs as compared to the power series-based solutions, in the whole spectra of the sizes of the PSC and ECC. In comparison to the other numerical approaches such as the finite element method, our method provides results with comparable accuracy but requires no pre-processing and post-processing and therefore is much more efficient. With the obtained solutions, we successfully predicted the critical pressure to break the annular ligament between the combo cracks. The results of this paper should be of general value to solving the related fracture and contact problems in a more precise and efficient way and deserve the inclusion by the updated solution handbook of cracks.

Appendix A. Determination of the simultaneous Fredholm integral equations

For the annular contact problem shown in Figure 1b, the pressure load is expressed as a piecewise function

$$f(r)=\begin{cases} p_0, & (0\le r\le d) \\ 0, & (d<r\le a) \end{cases} \tag{A1}$$

We follow the approach developed by Selvadurai and Singh (1987), in which the following auxiliary function $p_1(r)$ is introduced

$$p_1(r)=\frac{2}{\pi}\int_r^a\left\{\int_0^s\frac{tf(t)dt}{\left(s^2-t^2\right)^{1/2}}\right\}\frac{ds}{\left(s^2-r^2\right)^{1/2}} \tag{A2}$$

Substitution of Eq. (A1) into Eq. (A2) gives rise to

$$p_1(r)=\begin{cases} \dfrac{2}{\pi}p_0\left(a^2-r^2\right)^{1/2}-\dfrac{2}{\pi}p_0\displaystyle\int_d^a\frac{\left(s^2-d^2\right)^{1/2}}{\left(s^2-r^2\right)^{1/2}}ds, & (0\le r\le d) \\ \dfrac{2}{\pi}p_0\left(a^2-r^2\right)^{1/2}-\dfrac{2}{\pi}p_0\displaystyle\int_r^a\frac{\left(s^2-d^2\right)^{1/2}}{\left(s^2-r^2\right)^{1/2}}ds, & (d<r\le a) \end{cases} \tag{A3}$$

Inserting the above $p_1(r)$ into the general expression developed by Selvadurai and Singh (1987), the first equation of the pair of simultaneous Fredholm integral equations for our problem in Figure 1b is then given by

$$F_1(s)+\frac{2s}{\pi}\int_b^\infty\frac{F_2(u)du}{(u^2-s^2)}=\begin{cases} -p_0 s, & (0\le s\le d) \\ -p_0\left[s-\left(s^2-d^2\right)^{1/2}\right], & (d\le s\le a) \end{cases} \tag{A4}$$

while the second one is the same as that given by Selvadurai and Singh (1987) which is simply duplicated below for easy reference

$$F_2(s)+\frac{2}{\pi}\int_0^a\frac{uF_1(u)du}{(s^2-u^2)}=0, \quad (b\le s<\infty) \tag{A5}$$

Appendix B. Building functions of the power-series solutions to $\overline{\boldsymbol{F}}_{\mathbf{1}}$ and $\overline{\boldsymbol{F}}_{\mathbf{2}}$

$$m_1(\bar{s}) = 0\,,\ m_2(\bar{s}) = 0\,,\ m_4(\bar{s}) = 0$$

$$m_0(\bar{s}) = \begin{cases} -\bar{s}, & \left(0 \le \bar{s} \le \bar{d}\right) \\ -\bar{s} + \left(\bar{s}^2 - \bar{d}^2\right)^{1/2}, & \left(\bar{d} < \bar{s} \le 1\right) \end{cases}$$

$$m_3(\bar{s}) = -\frac{4\bar{s}}{9\pi^2}\phi_1\left(\bar{d}\right)$$

$$m_5(\bar{s}) = -\frac{4}{5\pi^2}\left[\frac{\bar{s}}{5}\phi_2\left(\bar{d}\right) + \frac{\bar{s}^3}{3}\phi_1\left(\bar{d}\right)\right]$$

$$m_6(\bar{s}) = -\frac{16\bar{s}}{81\pi^4}\phi_1\left(\bar{d}\right)$$

$$m_7(\bar{s}) = -\frac{4\bar{s}}{\pi^2}\left[\frac{1}{49}\phi_3\left(\bar{d}\right) + \frac{\bar{s}^2}{35}\phi_2\left(\bar{d}\right) + \frac{\bar{s}^4}{21}\phi_1\left(\bar{d}\right)\right]$$

$$m_8\left(\bar{s}\right) = -\frac{16}{\pi^4}\left[\frac{\bar{s}}{75}\phi_6\left(\bar{d}\right) + \frac{\bar{s}^3}{135}\phi_1\left(\bar{d}\right)\right]$$

$$n_0(\bar{s}) = 0\,,\ n_1(\bar{s}) = 0\,,\ n_3(\bar{s}) = 0$$

$$n_2(\bar{s}) = \frac{2}{3\pi\bar{s}^2}\phi_1\left(\bar{d}\right)$$

$$n_4(\bar{s}) = \frac{2}{5\pi\bar{s}^4}\phi_2\left(\bar{d}\right)$$

$$n_5(\bar{s}) = \frac{8}{27\pi^3\bar{s}^2}\phi_1\left(\bar{d}\right)$$

$$n_6(\bar{s}) = \frac{2}{7\pi\bar{s}^6}\phi_3\left(\bar{d}\right)$$

$$n_7(\bar{s}) = \frac{16}{\pi^3\bar{s}^2}\left[\frac{1}{75}\phi_4\left(\bar{d}\right) + \frac{1}{90\bar{s}^2}\phi_1\left(\bar{d}\right)\right]$$

$$n_8(\bar{s}) = \frac{2}{9\pi\bar{s}^2}\left\{\frac{16}{27\pi^4}\phi_1\left(\bar{d}\right) + \frac{1}{\bar{s}^6}\phi_5\left(\bar{d}\right)\right\}$$

In the above equations,

$$\phi_1\left(\bar{d}\right) = 1 - (1 - \bar{d}^2)^{3/2}$$

$$\phi_2\left(\bar{d}\right) = 1 - \frac{1}{3}(1 - \bar{d}^2)^{3/2}(3 + 2\bar{d}^2)$$

$$\phi_3\left(\bar{d}\right)=1-\frac{1}{15}\left(1-\bar{d}^2\right)^{3/2}(15+12\bar{d}^2+8\bar{d}^4)$$

$$\phi_4\left(\bar{d}\right)=\frac{\phi_1\left(\bar{d}\right)+\phi_2\left(\bar{d}\right)}{2}=1-\frac{1}{3}(1-\bar{d}^2)^{3/2}\left(3+\bar{d}^2\right)$$

$$\phi_5\left(\bar{d}\right)=1-\frac{1}{35}\left(1-\bar{d}^2\right)^{3/2}\left(35+30\bar{d}^2+24\bar{d}^4+16\bar{d}^6\right)$$

$$\phi_6\left(\bar{d}\right)=\frac{2}{3}\left[\phi_1\left(\bar{d}\right)+\frac{1}{2}\phi_2\left(\bar{d}\right)\right]=1-(1-\bar{d}^2)^{3/2}(1+\frac{2}{9}\bar{d}^2)$$

The functions ϕ_i $(i=1,2,\cdots,6)$ above reflect the effect of the size of the load region $\bar{d}$ on the results. It can be easily verified that $\phi_i=1$ $(i=1,2,\cdots,6)$ when $\bar{d}\rightarrow 1$.

Declaration of Competing Interest

The authors declare that they have no known competing financial interests or personal relationships that could have appeared to influence the work reported in this paper.

Acknowledgment

This work was partially supported by National Natural Science Foundation of China (Grant no. 11772283) and the Departmental General Research Fund of The Hong Kong Polytechnic University (G-YBXP).

References

Barenblatt, G.I., 1962. Mathematical theory of equilibrium cracks in brittle fracture. Advance in Applied Mechanics 7, 55-129.

Gladwell, G.M.L., 1980. Contact problems in the classical theory of elasticity. Sijthoff and Nooldhoff, Leyden.

Griffith, A.A., 1921. The phenomena of rupture and flow in solids. Phil. Trans. Roy. Soc. Lond. A 221, 163-198.

Israelachvili, J.N., 1992. Intermolecular and surface forces, 2nd ed. Academic Press, San Diego.

Kovvali, N., 2013. Theory and application of Gaussian quadrature methods. Morgan & Claypool.

Selvadurai, A.P.S., Singh, B.M., 1987. Axisymmetric problems for an externally cracked elastic solid. I. Effect of a penny-shaped crack. Int. J. Engng. Sci. 25, 1049-1057.

Sneddon, I.N., 1946. The distribution of stress in the neighborhood of a crack in an elastic solid. Proc. Roy. Soc. Lond. A 187, 229-260.

Sneddon, I.N., 1951. Fourier Transforms. McGraw Hill, New York.

Tada, H., Paris, P.C., Irwin, G.R., 2000. The stress analysis of cracks handbook. ASME Press, New York.

Yao, H., 2006. Mechanics of robust and releasable adhesion in biology (PhD thesis). Universität Stuttgart.